PAPER • OPEN ACCESS

Path Laplacians versus fractional Laplacians as nonlocal operators on networks

To cite this article: Ernesto Estrada 2021 *New J. Phys.* **23** 073049

New Journal of Physics
The open access journal at the forefront of physics

Deutsche Physikalische Gesellschaft DPG
IOP Institute of Physics

Published in partnership with: Deutsche Physikalische Gesellschaft and the Institute of Physics

OPEN ACCESS

RECEIVED
7 June 2021

REVISED
6 July 2021

ACCEPTED FOR PUBLICATION
14 July 2021

PUBLISHED
29 July 2021

PAPER

Path Laplacians versus fractional Laplacians as nonlocal operators on networks

Ernesto Estrada*

Institute for Cross-Disciplinary Physics and Complex Systems (IFISC, UIB-CSIC), Campus Universitat de les Illes Balears E-07122, Palma de Mallorca, Spain

* Author to whom any correspondence should be addressed.

E-mail: estrada@ifisc.uib-csic.es

Keywords: diffusion on networks, path-Laplacians, fractional Laplacian, spectral graph theory, cancer cell graphs

Abstract

Here we study and compare nonlocal diffusion processes on networks based on two different kinds of Laplacian operators. We prove that a nonlocal diffusion process on a network based on the path Laplacian operator always converges faster than the standard diffusion. The nonlocal diffusion based on the fractional powers of the graph Laplacian frequently converges slower than the local process. Additionally, the path-based diffusion always displays smaller average commute time and better diffusive efficiency than the local diffusive process. On the contrary, the fractional diffusion frequently has longer commute times and worse diffusive efficiency than the standard diffusion process. Another difference between the two processes is related to the way in which they operate the diffusion through the nodes and edges of the graph. The fractional diffusion occurs in a backtracking way, which may left the diffusive particle trapped just behind obstacles in the nodes of the graph, such as a weighted self-loop. The path-diffusion operates in a non-backtracking way, which may represent through-space jumps that avoids such obstacles. We show that the fractional Laplacian cannot differentiate between three classes of brain cellular tissues corresponding to healthy, inflamed and glioma samples. The path Laplacian diffusive distance correctly classifies 100% of the mentioned samples. These results illuminates about the potential areas of applications of both kinds of nonlocal operators on networks.

1. Introduction

Nonlocal interactions are ubiquitous in many physical and biological systems [1–5]. In general, the term 'nonlocal' is applied for large systems of interacting particles where a single particle can interact not only with its nearest neighbors but also with particles far away [6]. Many of these systems can be represented as networks in which the nodes describe the physical or biological entities and the edges represent their interactions [7–9]. Caution should be taken here to consider nonlocal interactions in network setting. Once two nodes are connected by an edge their interaction is considered to be local, although they can be geometrically separated at a long distance. Therefore, the nonlocal interaction in a network refers to the cases where a node 'feels' the influence of another which is not connected to it in the network. Such systems can be useful to represent for instance, swarms of insects, flocks of birds, schools of fish or colonies of bacteria in biology [3, 4], or the atoms/molecules adsorbed on the surface of metals, cold atomic clouds, natural light-harvesting complexes, helium Rydberg atoms, and cold Rydberg gases in physics [10]. All of them display long-range interactions of nonlocal character, which could display features that are not often observed in other systems, such as broken ergodicity and long-standing out-of-equilibrium regimes [11].

From a mathematical point of view these nonlocal behaviors are captured by nonlocal operators. In particular, for diffusion-like processes the fractional Laplacian [12] is frequently used. It can be represented

by a singular integral in real space $\mathbb{R}^d$:

$$(-\triangle)^s f(x) := C_{d,s} \int_{\mathbb{R}^d} \frac{f(x) - f(y)}{|x-y|^{d+2s}} \, dy, \tag{1.1}$$

where $f : \mathbb{R}^d \to \mathbb{R}$, $0 < s < 1$ and $C_{d,s} := \left(4^s \Gamma\left(d/2 + s\right)\right) / \left(\pi^{d/2} \left|\Gamma(-s)\right|\right)$ with $\Gamma(\cdot)$ as the gamma function. The nonlocal notion of derivative in the graph setting can be written as [13]:

$$\partial_y f(x) := \frac{f(y) - f(x)}{f\left(d(x,y)\right)}, \tag{1.2}$$

where $0 < f\left(d(x,y)\right) \leqslant \infty$ is a positive measure defined between the nodes x and y. In this framework, Estrada [14–16] proposed the path Laplacian operators for graphs which reads as

$$\left(\tilde{\mathcal{L}}_s f\right)(v) := \sum_{w \in V:\, d(v,w)=d} \frac{f(v) - f(w)}{d^s(v,w)}, \tag{1.3}$$

where $d(v,w)$ is the shortest path distance between the two nodes and $0 \leqslant s \leqslant \infty$ is the nonlocal parameter. The sum is carried out for all pairs of nodes which are at exactly the distance d from each other.

Another definition of the fractional Laplacian in the continuous setting is based on the spectrum of the operator [12]. In this case

$$(-\triangle)^\alpha v := \sum_{k=1}^{\infty} \lambda_k^\alpha (v, \phi_k) \phi_k, \tag{1.4}$$

where λ_k and ϕ_k are the eigenvalues and eigenvectors of $-\triangle$, Ω is a bounded Lipschitz domain, $v \in \left\{w \in L^2(\Omega) : (-\triangle)^s w \in L^2(\Omega)\right\}$, $(\cdot,\cdot)$ denotes the inner product in the L^2 Hilbert space, and $0 < \alpha < 1$. An adaptation of this definition to the case of the graph Laplacian was conducted by Riascos and Mateos [17, 18]. They defined the 'fractional' graph Laplacian as the fractional powers of the graph Laplacian $\mathcal{L}^\alpha := U\Lambda^\alpha U^{\mathrm{T}}$, where U is the matrix of orthonormalized eigenvectors and Λ the diagonal matrix of eigenvalues of the graph Laplacian [30–33]. Here $\mathcal{L} = K - A$, where K is a diagonal matrix of node degrees and A is the adjacency matrix of the graph.

So far the two approaches, the path Laplacians [14–16] and the fractional powers of the graph Laplacian [17, 18] (hereafter the fractional Laplacian) have grown independently in the literature. The first mainly in the mathematics and applications literature [19–24] and the second in the physics one [25–29]. However, there has not been a comparison between the two approaches that clarifies their physical meaning and areas of potential applicability. This is particularly true for the case of the fractional Laplacian for which no physical meaning, apart from its involvement in nonlocal random walks, has been given. In the case of the path Laplacian it is clear that the operator accounts for the hops of a diffusive particle between pairs of nodes of a graph with probabilities that decays as a function of the distance between the nodes. However, such interpretation does not exist, in a physical sense, for the spectral fractional graph Laplacian. For instance, for this operator we do not understand which law governs the particle hop between nodes, or how the fractional parameter influences the strength of the nonlocal over the local process.

Here we investigate both nonlocal Laplacian operators for networks. We focus in particular on their use in the graph nonlocal diffusion equation. We prove here that such nonlocal diffusion always converges faster when the path Laplacian is used than with the use of the local (standard) graph Laplacian. However, in the case of the fractional Laplacian the nonlocal diffusion converges slower than the local process if the algebraic connectivity of the graph is not smaller than one. We found that a nonlocal diffusive process controlled by the fractional Laplacian cannot overcome obstacles in the graph, such as a weighted self-loop at one node with a very high weight. On the contrary, we show here that such obstacle can be avoided via the through-space navigation used by the path Laplacian. We explain here why these situations occurs by finding a physical meaning for the nature of the diffusive processes controlled by these two operators on graphs. We also prove that the fractional Laplacian has longer commute times and worse diffusive efficiency than the standard diffusion process. As proved here, the path Laplacian always produces smaller commute times and better diffusive efficiencies than the standard Laplacian. Finally, we apply the two Laplacians to study the classification of brain cellular samples corresponding to healthy, inflamed and glioma tissues. We show that the fractional Laplacian cannot differentiate between the three classes while the path Laplacian diffusive distance is capable of correctly classifying 100% of the samples. We give a plausible explanation of the biological process possibly occurring in these three different kinds of cellular tissues.

2. *d*-path Laplacian operators

Let us fix any α with $0 < \alpha \leqslant \infty$ and let us define the matrix $M = \left[m_{ij}\right] : m_{ij} \in (-\alpha, \alpha)$ for all $i, j = 1, \ldots, n$. Let $\tilde{f}$ be a real function on the open interval $(-\alpha, \alpha)$. We define the pseudo-entrywise (pseudo-Hadamard) matrix function $\tilde{f}(M)$ as

$$\left(\tilde{f}(M)\right)_{ij} := \begin{cases} f\left(m_{ij}\right) & \text{if } m_{ij} \neq 0 \\ 0 & \text{if } m_{ij} = 0 \end{cases}. \tag{2.1}$$

Let $D = \left[d_{ij}\right]_{n \times n}$ be the shortest path distance matrix of the network G [9]. Then, let us define the pseudo-entrywise matrix functions of D as $\tilde{f}(D)$.

Here, the function f could be an exponential, a trigonometric function or simply the power function. Let us hereafter focus only on the negative power function, such that if $(-s)$ represents the entrywise power we define $\tilde{A}_s = \left[\tilde{a}_{ij}(s)\right]$ where

$$\tilde{a}_{ij}(s) := \begin{cases} d_{ij}^{-s} & \text{if } i \neq j, \\ 0 & \text{if } i = j. \end{cases} \tag{2.2}$$

It can be seen that $\tilde{A}_s$ is a generalized adjacency matrix from the fact that: $\lim_{s \to \infty} \tilde{A}(s) = A$. Let us now define the generalized node degree matrix as

$$\tilde{K}_s := \text{diag}\left(\tilde{A}_s \vec{1}^{\mathrm{T}}\right). \tag{2.3}$$

Therefore, we can define

$$\tilde{\mathcal{L}}_s := \tilde{K}_s - \tilde{A}_s, \tag{2.4}$$

as a generalization of the graph Laplacian matrix. This generalization considers the nonlocal interaction between a pair of nodes through a shortest path connecting them. For instance, the path Laplacian of a linear chain of 4 nodes labeled as 1–2–3–4 is:

$$\tilde{\mathcal{L}}_s = \begin{pmatrix} 1 + 2^{-s} + 3^{-s} & -1 & -2^{-s} & -3^{-s} \\ -1 & 2 + 2^{-s} & -1 & -2^{-s} \\ -2^{-s} & -1 & 2 + 2^{-s} & -1 \\ -3^{-s} & -2^{-s} & -1 & 1 + 2^{-s} + 3^{-s} \end{pmatrix}, \tag{2.5}$$

which indicates that the pairs of connected nodes in the graph interacts locally with 'strength' equal to one, and additionally the pairs $(1, 3)$ and $(2, 4)$ interact through nonlocal interactions with 'strength' 2^{-s}, while the pair $(1, 4)$ interacts nonlocally with 'strength' 3^{-s}. We can express these 'strength' in terms of probabilities by defining the transition matrix $\tilde{S}_s$ of the embedded Markov chain related to $\tilde{\mathcal{L}}_s$ (for reviews about random walks on graphs see [34–36] and for its connection with diffusion on networks see [37]). That is,

$$\tilde{S}_s = I - \left(\text{diag}\left(\tilde{\mathcal{L}}_s\right)\right)^{-1} \tilde{\mathcal{L}}_s. \tag{2.6}$$

Therefore, the probability that in the previous example a particle at node 1 at time t hops to node 2 at time $t + 1$ is $1/\left(1 + 2^{-s} + 3^{-s}\right)$, while for hopping to node 3 it is $2^{-s}/\left(1 + 2^{-s} + 3^{-s}\right)$, and to node 4 it is $3^{-s}/\left(1 + 2^{-s} + 3^{-s}\right)$. If $s = 2$ these probabilities are approx. 0.735, 0.184 and 0.082, indicating that the local hopping is more probable than that to a second neighbor and much more probable than to a third neighbor.

We can write down now the conservative equation of a diffusion process taking place on the nodes and edges of the network. Namely, if $\mathscr{D}$ is the diffusion coefficient [14–16], we have

$$\frac{\mathrm{d}x(G)}{\mathrm{d}t} = -\mathscr{D}\tilde{\mathscr{L}}_s \cdot x(t), \tag{2.7}$$

with initial condition $x(t = 0) = x_0$. The solution of (2.7) is given by

$$x(G) = \exp\left(-t\mathscr{D}\tilde{\mathscr{L}}_s\right) x_0. \tag{2.8}$$

We will consider hereafter $\mathscr{D} = 1$ for the sake of simplicity. The path time-evolution (path heat kernel) appearing in the solution of the path diffusion equation can be expressed as

$$\exp\left(-t\tilde{\mathcal{L}}_s\right) = \tilde{\psi}_1\tilde{\varphi}_1^{\mathrm{T}}\,\exp\left(-t\tilde{\mu}_1\right) + \tilde{\psi}_2\tilde{\varphi}_2^{\mathrm{T}}\,\exp\left(-t\tilde{\mu}_2\right) + \cdots + \tilde{\psi}_n\tilde{\varphi}_n^{\mathrm{T}}\,\exp\left(-t\tilde{\mu}_n\right), \tag{2.9}$$

where $\tilde{\psi}_j$ and $\tilde{\varphi}_j$ are the jth column of $U\left(\tilde{\mathcal{L}}_s\right)$ and of $U^{\mathrm{T}}\left(\tilde{\mathcal{L}}_s\right)$, respectively, and $0 = \mu_1 < \mu_2 \leqslant \cdots \leqslant \mu_n$. Then, we have

$$\lim_{t\to\infty}\exp\left(-t\tilde{\mathcal{L}}_s\right) = \tilde{\psi}_1\tilde{\varphi}_1^{\mathrm{T}}, \tag{2.10}$$

where $\tilde{\psi}^{\mathrm{T}}{}_1\tilde{\varphi}_1 = 1$. Let us take $\tilde{\psi}_1 = \frac{1}{\sqrt{n}}\vec{1}$, such that we have

$$\lim_{t\to\infty} x\left(t\right) = \lim_{t\to\infty}\left(\exp\left(-t\tilde{\mathcal{L}}_s\right)\right)x_0 = \frac{1}{\sqrt{n}}\left(\vec{1}\tilde{\varphi}_1^{\mathrm{T}}\right)x_0 = \frac{1}{\sqrt{n}}\left(\tilde{\varphi}_1^{\mathrm{T}}x_0\right)\vec{1} = \frac{\sum_{i=1}^{n}x_{0_i}}{n}. \tag{2.11}$$

Because $\mu_2\left(\tilde{\mathcal{L}}_s\right)$ makes the largest contribution to $\exp\left(-t\tilde{\mathcal{L}}_s\right)$ among all the nonzero eigenvalues of $\tilde{\mathcal{L}}_s$, it dictates the rate of convergence of the diffusion process.

The following result has not been previously noticed in the literature about the path Laplacians of graphs. Let $G = (V, E)$ be a simple connected graph different from the complete graph. Let $\tilde{\mathcal{L}}_s\left(G\right)$ be the path Laplacian of G. Then, $\tilde{A}_s$ is the adjacency matrix of a weighted complete graph $\tilde{K}_n$. It is known that the algebraic connectivity [39–41] is a nondecreasing function of each edge weight [38]. Then, if we reduce the weights of the edges the algebraic connectivity will not increase. We have seen that $\mathcal{L}\left(G\right) = \lim_{s\to\infty}\tilde{\mathcal{L}}_s\left(G\right)$, which corresponds to the algebraic connectivity of the network [39–41], therefore as $s \to \infty$ implies reducing the edge weights we have that

$$\mu_2\left(\mathcal{L}\left(G\right)\right) \leqslant \mu_2\left(\tilde{\mathcal{L}}_s\left(G\right)\right). \tag{2.12}$$

This result implies that a diffusive process controlled by the path Laplacian never converges at a slower rate than a similar process controlled by the local Laplacian. Also important is the fact that as we increase the nonlocal effect in a graph by reducing s, we are accelerating the convergence of the process. That is, a diffusion on a graph will converge faster when $s = 2$ than when $s = 4$, where the first represents a stronger long-range (nonlocal) interactions.

Finally, note that both processes converges to each other when $s \to \infty$, i.e. when no nonlocal interactions are taken into account:

$$\lim_{s\to\infty} x\left(G\right) = \lim_{s\to\infty}\exp\left(-t\tilde{\mathcal{L}}_s\right)x_0 = \exp\left(-t\mathcal{L}\right)x_0. \tag{2.13}$$

2.1. General properties of the path Laplacians

From a physical point of view we should obtain the Laplacian from the divergence of the gradient of a function defined on the set of nodes of the graph. Then, let us define such a path gradient matrix, $\nabla\left(s\right) \in \mathbb{R}^{p\times n}$, of a connected graph of n nodes, where $p = n\left(n-1\right)/2$. Let $l_{i,j}$ be a shortest path of length d_{ij} connecting the nodes i and j. Let us replace the shortest path $l_{i,j}$ by an arbitrarily directed edge $e = \left(i, j\right)$. Let e has a weight d_{ij}^{-s}. Then,

$$\nabla_{e,v}\left(s\right) = \begin{cases} -d_{ij}^{-(s/2)} & \text{if node v is the head of the edge e,} \\ d_{ij}^{-(s/2)} & \text{if node v is the tail of the edge e,} \\ 0 & \text{otherwise.} \end{cases} \tag{2.14}$$

It is straightforward to realize that, as desired:

$$\tilde{\mathcal{L}}_s = \nabla^{\mathrm{T}}\left(s\right)\nabla\left(s\right). \tag{2.15}$$

Let $\ell^2(V)$ be the Hilbert space of functions on V with inner product (see [4, 42])

$$\langle f, g\rangle = \sum_{v\in V} f(v)\overline{g(v)}, \quad f, g \in \ell^2(V). \tag{2.16}$$

The path Laplacian is then defined as the following operator in $\ell^2(V)$

$$\left(\tilde{\mathcal{L}}_s f\right)(v) := \sum_{w\in V:\, d(v,w)=d} \frac{f(v)-f(w)}{d^s(v,w)}, \quad f\in \ell^2(V). \tag{2.17}$$

When $s\to\infty$ it transforms into

$$\left(\mathcal{L} f\right)(v) := \sum_{(v,w)\in E} f(v)-f(w), \quad f\in \ell^2(V), \tag{2.18}$$

which is the definition of the standard Laplacian.

Finally, let us define the following matrices $\mathcal{L}_d = \left[\mathcal{L}_d(i,j)\right]$ where

$$\mathcal{L}_d(i,j) = \begin{cases} \delta_i & \text{if } i=j, \\ -1 & \text{if } d_{ij}=d, \\ 0 & \text{otherwise,} \end{cases} \tag{2.19}$$

where $\delta_d(v)$ is the d-path degree of a vertex $v\in V$:

$$\delta_d(v) = \#\{w\in V : d(v,w)=d\}. \tag{2.20}$$

Obviously, $\mathcal{L}_1=\mathcal{L}$. Then, $\tilde{\mathcal{L}}_s$ can be written as

$$\tilde{\mathcal{L}}_s = \sum_{d=1}^{\triangle} d^{-s}\mathcal{L}_d = \mathcal{L} + \sum_{d=2}^{\triangle} d^{-s}\mathcal{L}_d, \tag{2.21}$$

where $\triangle$ is the diameter of the graph. This last formulation allows us to introduce a subtle but important modification. That is, we can make the nonlocal parameter s also dependent on the shortest-path distance separating the interacting nodes. In this case we have

$$\tilde{\mathcal{L}}_s = \mathcal{L} + \sum_{d=2}^{\triangle} d^{-s_d}\mathcal{L}_d, \tag{2.22}$$

where s_d is any real function on d. Suppose, for instance, that we need to eliminate the hopping between nodes at a given shortest path distance equal to ζ, while the rest of interactions decay as d^{-2}. We can then use:

$$s_d = \begin{cases} \infty & \text{if } d=\zeta \\ 2 & \text{if } d\neq\zeta. \end{cases} \tag{2.23}$$

3. Fractional powers of the graph Laplacian

Riascos and Mateos [17, 18] considered the fractional powers of the Laplacian matrix L^α as an operator for describing nonlocal interactions on graphs. The fractional powers of the Laplacian matrix can be defined by using the following integral [43]:

$$\mathcal{L}^\alpha := \frac{\sin(\alpha\pi)}{\alpha\pi}\mathcal{L}\int_0^\infty \left(t^{1/\alpha}I+\mathcal{L}\right)^{-1} \mathrm{d}t. \tag{3.1}$$

In practice it can be obtained through the spectral decomposition of the Laplacian as: $\mathcal{L}^\alpha = U\Lambda^\alpha U^{\mathrm{T}}$. They considered the 'fractional' diffusion equation of a graph G to be [17, 18]:

$$\frac{\mathrm{d}x(G)}{\mathrm{d}t} = -\mathcal{L}^\alpha\cdot x(t), x(0)=x_0, \tag{3.2}$$

whose solution is given by $x(t)=e^{-t\mathcal{L}^\alpha}x_0$. Similar as we did for the case of path diffusion equation we can express the fractional time-evolution (fractional heat kernel) as

$$\exp\left(-t\mathcal{L}^\alpha\right) = \psi_1\varphi_1^{\mathrm{T}}\exp\left(-t\mu_1^\alpha\right) + \psi_2\varphi_2^{\mathrm{T}}\exp\left(-t\mu_2^\alpha\right) + \cdots + \psi_n\varphi_n^{\mathrm{T}}\exp\left(-t\mu_n^\alpha\right), \tag{3.3}$$

where ψ_j and φ_j are the jth column of $U(\mathcal{L})$ and of $U^{\mathrm{T}}(\mathcal{L})$, respectively. Following a similar procedure as before we can show that the process converges and that $\mu_2(\mathcal{L}^\alpha)$ dictates the rate of convergence of the diffusion process. This indicates that the larger the value of the first nonzero eigenvalue of $\mathcal{L}^\alpha$ the faster the convergence of the diffusive process.

Let us then show a result that has not been previously discussed in the literature about the fractional powers of the Laplacian matrix. Let G be a graph having $\mu_2(\mathcal{L}) > 1$ then $\mu_2(\mathcal{L}^\alpha) < \mu_2(\mathcal{L})$ indicating that the fractional diffusive process will converge more slowly than the local diffusive one. Let us consider, for instance, an Erdös–Rényi random graph $G(n,p)$, i.e. a random graph with n nodes and linking probability p [44]. Then,

$$\mu_2\left(\mathcal{L}\left(G\left(n,p\right)\right)\right) = pn + o\left(n^{1/2+\epsilon}\right), \tag{3.4}$$

which converges in probability as $n \to \infty$ [45]. For an Erdös–Rényi random graph to be connected it is necessary that $pn > 1$ [44], which immediately implies that $\mu_2\left(\mathcal{L}^\alpha\left(G\left(n,p\right)\right)\right) < \mu_2\left(\mathcal{L}\left(G\left(n,p\right)\right)\right)$ for any value of α. It should be noticed that even in the case of $\mu_2(\mathcal{L}) < 1$ the convergence could be slower using the fractional Laplacian than using the local one. But this indicator of $\mu_2(\mathcal{L}) > 1$ serves to guarantee that at least in a few graphs the convergence of the fractional process is slower than the local one.

Here again we can obtain an embedded Markov chain whose transition matrix is given by

$$S(\mathcal{L}^\alpha) = I - \left(\mathrm{diag}\left(\mathcal{L}^\alpha\right)\right)^{-1}\mathcal{L}^\alpha. \tag{3.5}$$

Because $\mathcal{L}^\alpha_{vw} = (\mathcal{L}^\alpha)_{vw} = \sum_{j=1}^n \Psi_{jv}\Psi_{jv}\lambda_j^\alpha$ we can write $S_{vw}(\mathcal{L}^\alpha)$ for $v \neq w$ as

$$S_{vw}(\mathcal{L}^\alpha) = \frac{\sum_{j=1}^n \Psi_{jv}\Psi_{jw}\lambda_j^\alpha}{\sum_{j=1}^n \Psi_{jv}^2\lambda_j^\alpha}, \tag{3.6}$$

and zero for the main diagonal entries.

4. Comparing path Laplacians and fractional graph Laplacians

4.1. The 'power series' representations

We first start by analysis of the operator $\mathcal{L}^\alpha$. We will focus here on $\mathcal{L}^{1/2}$ for the sake of simplicity. Because $\mathcal{L} \succeq 0$ (it is positive semi-definite) we have that $\left\|I - \frac{\mathcal{L}}{\|\mathcal{L}\|}\right\| \leqslant 1$, which implies that $\left\|\left(I - \frac{\mathcal{L}}{\|\mathcal{L}\|}\right)^k\right\| \leqslant \left\|I - \frac{\mathcal{L}}{\|\mathcal{L}\|}\right\|^k \leqslant 1$. Therefore we can write

$$\mathcal{L}^{1/2} := I - \sum_{k=1}^{\infty}\binom{1/2}{k}(I-\mathcal{L})^k. \tag{4.1}$$

The term $(I-\mathcal{L})^k$ can be written as $(B+A)^k$, where $B = I - K$ and A is the adjacency matrix. Then, it is clear that the power-series expansion of $\mathcal{L}^{1/2}$ contains a sum of powers of the adjacency matrix. The entries of these powers of the adjacency matrix are interpreted as follow. The term $\left(A^k\right)_{vw}$ counts the number of walks of length k between the nodes v and w of G. A *walk* of length k in G is a set of nodes $i_1, i_2, \ldots, i_k, i_{k+1}$ such that for all $1 \leqslant l \leqslant k$, $(i_l, i_{l+1}) \in E$. A *closed walk* is a walk for which $i_1 = i_{k+1}$. Therefore, a particle diffusing on G as described by $\mathcal{L}^{1/2}$ is hopping back and forth between two nodes before it arrives at its destination. Let us consider the term $(I-\mathcal{L})^2$ as an illustration. This term can be written as

$$(I-\mathcal{L})^2 = -2\mathcal{L} + \left(I + K^2 - KA - AK + A^2\right). \tag{4.2}$$

Let us focus only on the term A^2 (the rest will be analyzed later on). Here, $\left(A^2\right)_{vv}$ counts the number of backtracking (closed) walks of length 2 starting (and ending) at the node v. The term $\left(A^2\right)_{vw}$ is the only one accounting for a nonlocal interaction, as it describes the hops from a node v to a node w two edges apart from v.

Let us now move to the path-Laplacian operators. In order to express the path Laplacian matrix in terms of powers of the adjacency matrix we need to use a different kind of algebra. We define it as follows. Let $\left(\mathbb{R}\cup\{+\infty\},\oplus,\otimes\right)$ be the min tropical semiring with the operations [46–48]:

$$\begin{aligned} x\oplus y &:= \min\{x,y\},\\ x\otimes y &:= x+y. \end{aligned} \tag{4.3}$$

The identity element for $\oplus$ is $+\infty$ and that for $\otimes$ is 0. Then, we can define the tropical adjacency matrix power as

$$A^{\otimes k+1} = A^{\otimes k}\otimes A, \tag{4.4}$$

where $A^{\otimes 0}=\widehat{I}$, which is the tropical identity matrix, i.e. a matrix with zeros in the main diagonal and ∞ outside it.

We can now write the path Laplacian in terms of tropical powers of the adjacency matrix as:

$$\tilde{\mathcal{L}}_s = \text{diag}\left(\left(\bigoplus_{k=0}^{\infty} A^{\otimes k}\right)^{(-s)}\cdot\vec{1}\right) - \left(\bigoplus_{k=0}^{\infty} A^{\otimes k}\right)^{(-s)}, \tag{4.5}$$

where $(-s)$ represents the pseudo-Hadamard fractional powers of the corresponding matrix. The tropical sum is carried out up to infinity as it converges in all cases where there are no negative cycles in the graph. A negative cycle is a cycle where the product of the weights of all its edges is negative. Typically, except for signed graphs, we consider positive edge weights, which always avoid such negative cycles. The infinite sum $\oplus_{k=0}^{\infty}A^{\otimes k}$ is known as the Kleene star operator of A [46–48].

Therefore, the path Laplacians are based on the pseudo-Hadamard fractional powers of the tropical power-series (Kleene star) of the adjacency matrix. Let us recall that a *path* is a walk with no repeated nodes and edges. This means that $\tilde{L}_s$ accounts for nonbacktracking walks of minimum length, i.e. shortest paths, between the corresponding pairs of nodes. In contrast, L^{α} accounts for backtracking walks of any length between the pairs of nodes.

4.2. Backtracking vs non-backtracking nonlocal diffusion

To start our comparison here we will focus on the complete graph K_n with n nodes. In this case, the fractional powers of the Laplacian can be written as

$$\left(\mathcal{L}^{\alpha}\left(K_n\right)\right)_{pq} = \begin{cases} n^{\alpha}-n^{\alpha-1} & p=q,\\ n^{\alpha-1} & p\neq q. \end{cases} \tag{4.6}$$

This means that the fractional powers of the Laplacian of a complete graph changes with the strength of the long-range interactions, although such nonlocal interactions do not exist in K_n, i.e. a diffusive particle in K_n can only jump to nearest neighbors. To be clearer, let $x\left(t=0\right)=[1,0,\ldots,0]^{\text{T}}$ (it is the same to start the process from any other node as all are equivalent). Then,

$$x\left(t\right) = \left[\frac{1+\left(n-1\right)e^{-tn^{\alpha}}}{n}, \frac{1-e^{-tn^{\alpha}}}{n},\ldots,\frac{1-e^{-tn^{\alpha}}}{n}\right]^{\text{T}}. \tag{4.7}$$

Obviously $x\left(K_n,t,\alpha=1\right)\neq x\left(K_n,t,\alpha\neq 1\right)$, which means that the local and the nonlocal versions of the same model are different for a complete graph.

The difference of particle concentrations between the node 1 and any other node is $\triangle_{1j}=e^{-tn^{\alpha}}$. Therefore, when $\alpha=1$ and n is sufficiently large, this difference is very close to zero. For instance, for only $n=10$ nodes the particle concentration at the starting point is 0.100 04, and at any other node it is 0.099 99 at $t=1$. However, if $\alpha\ll 1$ the difference of concentrations is significantly more marked between the starting point and any other node. For instance, for the same graph as before with $\alpha=0.25$ the concentrations are 0.2520 in the starting point and 0.0831 at any other node at $t=1$. This means that at the same time there is significantly higher concentration at the initial point than at the rest of the nodes. It is like if the particles were retained at the starting point and slowly propagate to the rest of the graph.

In order to understand the physical process that the fractional Laplacian produce when used in the graph diffusion equation we proceed by discretizing the time of the process. Let i be a node of the network and let $\epsilon>0$ be the step size. Then, the standard graph diffusive process can be written in terms of the discrete time k as [49]

$$x_i\left(k+1\right) = x_i\left(k\right) + \epsilon\sum_{(i,j)\in E} A_{ij}\left(x_j\left(k\right)-x_i\left(k\right)\right). \tag{4.8}$$

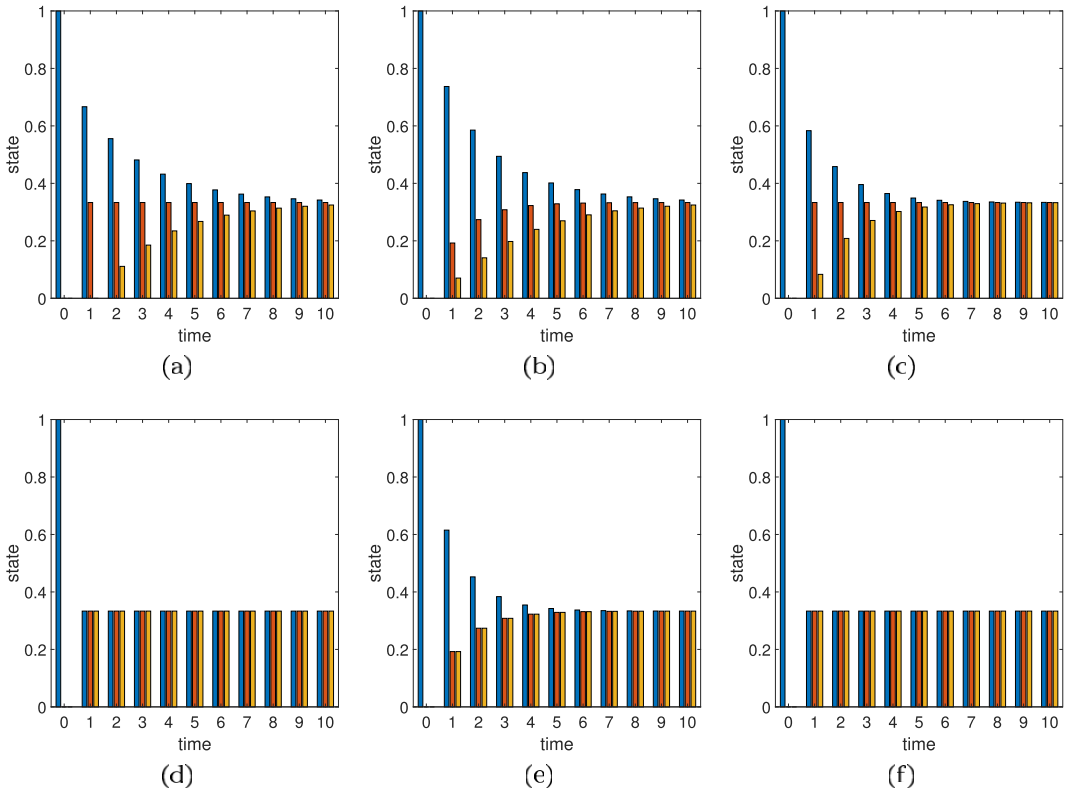

Figure 1. Bar plots of the state (concentration) of a diffusive particle at the different nodes of a linear chain with 3 nodes (a)–(c) and in a triangle (d)–(f). The plots correspond to the use of the three different Laplacian $\mathcal{L}$ (a), (d), $\mathcal{L}^{\alpha}$ (b), (e) and $\tilde{\mathcal{L}}_s$ (c), (f). In all cases we use $\alpha = 1/2$ and $s = 2$.

In matrix-vector form it is written as

$$x(k+1) = Px(k), \tag{4.9}$$

where $P = I - \epsilon\mathcal{L}$ is the Perron matrix [49]. We then generalize this process to include the fractional Laplacian and the path-Laplacians by using $P_f = I - \epsilon_f\mathcal{L}^{\alpha}$ and $\tilde{P}_s = I - \tilde{\epsilon}\tilde{\mathcal{L}}_s$, respectively. The values of the time step are $1/(1+\Xi)$ where Ξ is the maximum of all diagonal entries of the corresponding Laplacian, i.e. $\mathcal{L}$, $\mathcal{L}^{\alpha}$ and $\tilde{\mathcal{L}}_s$, respectively. For the sake of the current analysis we use $\alpha = 1/2$ and $s = 2$.

In figures 1(a)–(c) we illustrate the discrete time evolution of diffusive processes with the three Laplacians considered, i.e. $\mathcal{L}$, $\mathcal{L}^{\alpha}$ and $\tilde{\mathcal{L}}_s$, in a linear chain of three nodes. The standard diffusive process (figure 1(a)) using $\mathcal{L}$, proceeds as follows. At time zero all the particle concentration is at node 1 (blue bar). At time $t = 1$, part of this concentration is transferred to node 2, while the rest remains at the node 1. Then, at time $t = 2$ some concentration is transferred from node 2 to 3, while node 1 again transfers some concentration to node 2. The process continues in a similar fashion until equilibration. The main difference with the two nonlocal processes is that, in the last one at $t = 1$ node 1 transfers simultaneously some concentration to nodes 2 and 3. In the process with the fractional Laplacian it seems like if less concentration is transferred from node 1 to nodes 2 and 3, in relation to the process controlled by $\tilde{\mathcal{L}}_s$. The consequence of this difference is that the process controlled by the path-Laplacian arrives at equilibration faster than that controlled by $\mathcal{L}^{\alpha}$. It seems like if this were only a quantitative difference, but let us explore a complete graph to see whether these differences are also in the kind of mechanism behind these processes. In the appendix we also illustrate the results for a path (linear chain) of 100 nodes.

We now consider the evolution of the three diffusive processes in a triangle graph (figures 1(d)–(f)). In the appendix we so for a complete graph with 100 nodes. Because in this graph every pair of nodes is connected, the standard diffusive process evolves by transferring 1/3 of concentration from node 1 to nodes 2 and 3 at $t = 1$. Therefore, at this time the process arrives at the steady state as can be seen in figure 1(d). The same happens for the process controlled by $\tilde{\mathcal{L}}_s$ as can be seen in figure 1(e). The reason is that there are no longer-than-one steps in this complete graph as for the particle to evolve in a different manner as for the standard Laplacian. However, as can be seen in figure 1(e) when the process is controlled by the fractional Laplacian, at $t = 1$ only 1/5 of the concentration originally at node 1 is transferred to node 2, and a similar

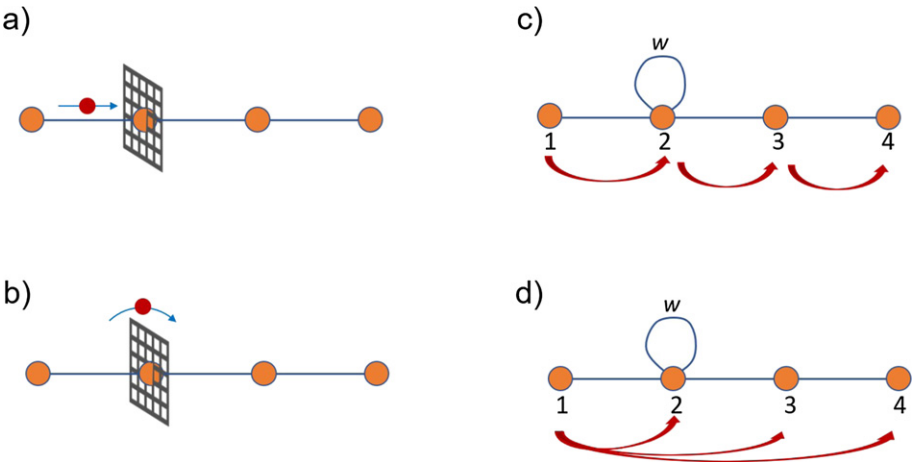

Figure 2. Schematic representation of a diffusive process across a linear chain of 4 nodes in which a membrane is located at one node, when there are local-only or through-edges nonlocal (a) and (c) and through-space nonlocal (b) and (d) interactions. Representation of the systems (a) and (b) in the form of a graph with a self-loop and the kind of hops expected in them. The parameter w represents the shielding capacity of the membrane.

amount to node 3. Then, the process continues until equilibration. But if there are no nonlocal interactions in this graph why this difference in the concentrations at the three nodes at $t = 1$?

To understand what is happening we should go back to the Taylor series expansion of the fractional powers of $\mathcal{L}$. Here again we focus on the particular case of $\mathcal{L}^{1/2}$ for the sake of simplicity. As we have seen the power $(I - \mathcal{L})^2$ contains the terms $I + K^2 + A^2 - KA - AK$. The terms $\left(I + K^2 + A^2\right)_{vv}$ accounts for closed walks of length two retaining the diffusive particle at the node v. The terms $-(KA + AK)_{vw}$, accounts for the movement of the diffusive particle from v to w, but just in case that the two nodes are connected. That is, this term only accounts for a local hop of the diffusive particle from one node to its nearest neighbors. Consequently, all the terms $\left(I + K^2 + A^2\right)_{vv}$ and $-(KA + AK)_{vw}$, are just trapping the particle either at the origin (node v) or at its closest environment, i.e. its nearest neighbors. Only the term $\left(A^2\right)_{vw}$ moves the particle nonlocally. This situation resembles a particle that departs a node and bounces back and forth before reaching its steady state. In the case of a complete graph like the triangle illustrated in figure 1(e), the particle departs from the origin node and visits all its nearest neighbors, but then it rebounds back to the origin where it is retained for a while. The backtracking diffusive process continues until equilibration is reached. On the contrary, in the process controlled by the path-Laplacian the diffusive particle departs from the origin and arrives at every nearest neighbor without bouncing back to the origin. This implies the equilibrium in just one step. As we will see this difference between backtracking and non-backtracking diffusion will have significant consequences for networks with self-loops.

4.3. Behavior in graphs 'with traps'

Let us simulate a situation in which a particle is hopping through the nodes of a linear chain in which we have placed a 'potential barrier' in one of the nodes as illustrated in figures 2(a) and (b) for the cases where there is not nonlocal hops (a) and where such nonlocal interactions are present (b). The potential barrier is represented here by a weighted self-loop at the node i as illustrated in figures 2(c) and (d), which corresponds to the cases illustrated in (a) and (b), respectively. The height of the barrier is $w \in \mathbb{R}^+$, which is then used as the weight for a self-loop located at the node i. That is, when $w = 0$ there is no barrier and the diffusion occurs without any 'obstacle' at the node i. We then simulate the diffusion of the particle from a node by using the local, fractional and path Laplacian matrices.

The results of the simulations using (i) $x(t) = \exp(-t\mathcal{L}) \cdot x_0$, (ii) $x(t) = \exp\left(-t\mathcal{L}^{1/2}\right) \cdot x_0$ and (iii) $x(t) = \exp\left(-t\tilde{\mathcal{L}}_s\right) \cdot x_0$ with initial condition $x_0 = [1, 0, 0, 0]^{\mathrm{T}}$, are illustrated in figure 3. We consider the processes at the very early time $t = 1$. However, the results are similar for other times in which the system is far from the steady state. In figure 3 we plot the results for the nodes 3 (a) and 4 (b) using $0 \leqslant w \leqslant 10,000$. As can be seen in the case of local-only interactions (i) we observe the expected continuous decay of the concentrations at nodes 3 and 4 with the height of the barrier at the node 2. In this case, as illustrated in figures 3(a) and (b) (blue circles), the concentration decays as a power-law with w: $x(G, t) \sim w^{-\gamma}$, where $\gamma > 0$ is a fitting parameter. In the case of the fractional Laplacian (ii) we observe in figures 3(a) and (b) (red squares) a behavior very similar to that of the local operator. Finally, when we consider the path Laplacian operator (iii) we see that at relatively low values of w, there is a small decay of the concentration

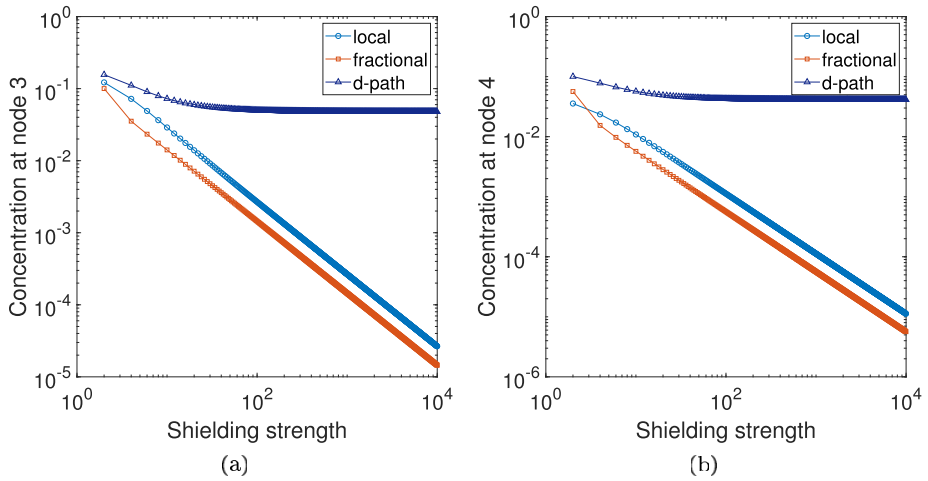

Figure 3. Change of the concentration at the nodes 3 (a) and 4 (b) in a linear chain with four nodes in which the particle starts at node 1 (see figure 2 for node labeling). (Blue) circles represents the case (i), (red) squares represents the use of the fractional powers of the Laplacian matrix (case (ii)) (we considered $\alpha = 1/2$) and (magenta) triangles represents the use of the d-path Laplacian operator (we used $s = 2$). See text for details.

at the nodes 3 and 4 (see figures 3(a) and (b) (triangles)), which then becomes constant at relatively large values of w. In the simulations we have used $s = 2$. For values $s > 2$ the curves converges to that of the nonlocal (standard) Laplacian. For values of $s < 2$ the convergence to the constant value is faster than that shown for $s = 2$.

To understand the effects of this barrier let us analyze first the case without nonlocal interactions. Suppose that the particle is diffusing from the node 1 on a linear chain of 4 nodes. With probability 1 at discrete time $k = 1$ the particle will move to node 2. When $w = 0$ (no barrier) the particle will have probability equal to $1/2$ to escape from that node (either to node 1 or to 3). However, such probability is $1/(2 + w)$ when we have placed the a barrier of height w. If the height of the barrier is high, the probability that a particle located at node 2 can hop to node 3 (or to node 1) is practically null, which makes the particle to get trapped between the node 1 and the node having the barrier.

Let us now consider the nonlocal scenarios. In these cases due to nonlocality at discrete time $k = 1$ the particle will populate nodes 2, 3 and 4 with probabilities that decay with their separation from node 1. In the case of the fractional Laplacian it is obvious from the previous results that the particle is not able to overcome the potential barrier. The reason for this behavior can be explained from the contributions of the terms having the form $\left(I + K^2 + A^2\right)_{vv}$. That is, in the fractional Laplacians there are terms contributing to retain the particle at a given node. Therefore, if the degree of the node is too high, such retention can trap the particle at the corresponding node for long time. As we have created a node with extremely high degree w, i.e. the potential barrier, the trapping of the particle at the self-loop is obvious. Additionally, the backtracking nature of the diffusive process controlled by this Laplacian also plays a role in trapping the particle behind the membrane. In this case the contribution of the term $-(KA + AK)_{1,2}$ accounts for the bouncing of the particle between the origin and the place where the barrier is locate. Because $k_w = w + 2$, when w is very high the particle remains bouncing back and forth for an extremely long period of time between these two nodes. All in all, the particle gets trapped between the origin and the potential barrier.

In the case of the path Laplacians it is evident from our results that the particle is able to overcome the potential barrier. We can think of several physical scenarios in which this situation occurs. For instance, (i) the particle is very energetic as to go over the potential; (ii) the particle navigates by a combination of 'through-edges' (which will encounter the barrier) and 'through-space' navigation (which avoids the barrier); (iii) a switching potential that allows the pass of certain class of particles like the one describe by the path Laplacian. These scenarios are compatible with the observation that the concentration of the particle at nodes 3 and 4 (see figure 3) first decay with the increase of w before it stabilizes at a constant value. For instance, we can suppose that $w < 20$ the through-edges navigation dominates, but when the barrier height is relatively large ($w > 20$), the through-space jumps from 1 to 3 and from 1 to 4 dominate over the through edges transitions: 1–2–3 and 1–2–3–4. At this point the concentrations at nodes 3 and 4 remain constant because they are mainly maintained by the long-jumps and not by the through-edges hops. Mathematically, this behavior is a consequence of the fact that this operators does not produce backtracking of the diffusive particle between the nodes, which avoid that it gets trapped.

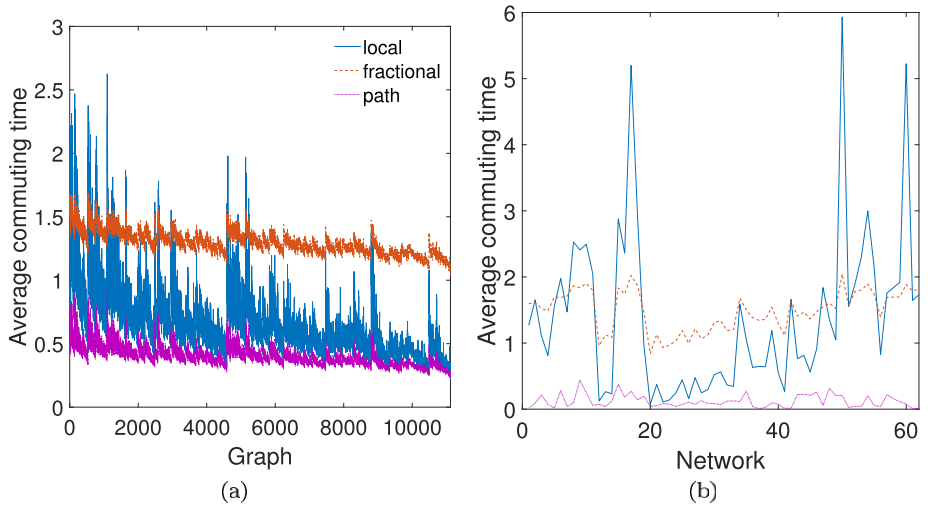

Figure 4. Plot of the average commute time of all connected graphs with 8 nodes (a) and of 62 real-world networks (b). The 62 real-world networks represent a wide variety of complex systems, e.g. social, ecological, biomolecular, infrastructural and informational (see Appendix in [9] for description and references). The continuous (blue) line corresponds to the distance based on local (standard) Laplacian, the broken (red) line to the one based on the fractional Laplacian and the dotted (magenta) line to the one based on the path Laplacian.

4.4. Commuting times

As we have seen before we can generate random walk processes based on the different Laplacians studied here via the embedded Markov chain. That is,

$$S\left(\mathscr{L}\right) = I - \left(\mathrm{diag}\left(\mathscr{L}\right)\right)^{-1}\mathscr{L}. \tag{4.10}$$

where $\mathscr{L} = \left\{\mathcal{L}, \mathcal{L}^{\alpha}, \tilde{\mathcal{L}}_{s}\right\}$. An important quantity in the study of random walks on graphs is the access or hitting time $\mathcal{H}\left(v,w\right)$, which is the expected number of steps before node w is visited, for a random walk starting at node v. The sum $\mathcal{C}\left(v,w\right) = \mathcal{H}\left(v,w\right) + \mathcal{H}\left(w,v\right)$ is called the commute time, which is the expected number of steps in a random walk starting at v, before node w is visited and then the walker comes back again to node v [34]. Then, in a simple graph the expected commuting time between a pair of nodes v and w can be expressed by

$$\mathcal{C}_{vw} = 2m\Omega_{vw}\left(\mathscr{L}\right), \tag{4.11}$$

where

$$\Omega_{vw}\left(\mathscr{L}\right) = \sum_{j=2}^{n}\frac{1}{\lambda_{j}\left(\mathscr{L}\right)}\left(\psi_{jv} - \psi_{jw}\right)^{2} \tag{4.12}$$

is the resistance distance between the corresponding pair of nodes [50–55]. As we are interested in global properties of the networks we study here the average resistance distance between every pair of nodes, $\left\langle\Omega\left(\mathscr{L}\right)\right\rangle = \frac{2}{n(n-1)}\sum_{v,w}\Omega_{vw}\left(\mathscr{L}\right)$. The sum of all resistance distances in a graph is known as the Kirchhoff index and is expressed in terms of the eigenvalues of the corresponding Laplacian as [51, 56–58]:

$$Kf\left(\mathscr{L}\right) = \sum_{v,w}\Omega_{vw}\left(\mathscr{L}\right) = 2n\sum_{j=2}^{n}\frac{1}{\lambda_{j}\left(\mathscr{L}\right)} = 2n\,\mathrm{tr}\left(\mathscr{L}^{+}\right), \tag{4.13}$$

where $\mathrm{tr}\left(\mathscr{L}^{+}\right)$ is the trace of the Moore–Penrose pseudoinverse of $\mathscr{L}$.

We first calculate the average commute times for all 11 117 connected graphs with 8 nodes. For the fractional Laplacians we used the values of $\alpha = 0.5$, $\alpha = 0.25$, and $\alpha = 0.01$. For the path Laplacians we study the cases $s = \{3,2,1\}$. First, we compare the average commuting times of random walks based on the local $\mathcal{L}$ and on fractional $\mathcal{L}^{\alpha}$ Laplacians. For $\alpha = 0.5$ we found that only in 229 graphs out of 11 117 (2.06%) the average commuting time is smaller for the fractional than for the local process. That is, in 97.94% of the graphs, a random walk based on local-only Laplacian displays smaller commute time than that based on $\mathcal{L}^{\alpha=0.5}$. When $\alpha = 0.25$ only 136 graphs (1.22%) display smaller commute time with the fractional than with the local Laplacian. These results are illustrated in figure 4(a). The situation is even worse for smaller values of α. For instance, for $\alpha = 0.01$ there are only 64 graphs (0.58%) for which the fractional Laplacian represents an improvement in the commute time. That is, in general, a random walk based on the fractional Laplacian does not improve the commuting time between pairs of nodes, but, on the

contrary, it makes this time longer. Additionally, the smaller the fractional power, the smaller the fraction of graphs which are benefited by such fractional random walks.

An analysis of the Kirchhoff index suggest that because $0 < \lambda_2(\mathcal{L}) \leqslant \cdots \leqslant \lambda_n(\mathcal{L})$, when $\lambda_2(\mathcal{L}) \geqslant 1$ the average commute time based on the local Laplacian is smaller than that based on the fractional Laplacian for any α. There are 6803 graphs for which this condition is obeyed among the 11 117 connected graphs with 8 nodes. Then, it is obvious that also for many graphs having $\lambda_2(\mathcal{L}) < 1$ the commute time based on local Laplacian is smaller than that based on the fractional one. We also consider here 62 real-world networks representing a wide variety of complex systems, e.g. social, ecological, biomolecular, infrastructural and informational (see appendix in [9] for description and references). In these networks we found that $\left\langle \Omega\left(\mathcal{L}^{3/4}\right)\right\rangle > \langle \Omega(\mathcal{L})\rangle$ in 35, $\left\langle \Omega\left(\mathcal{L}^{1/2}\right)\right\rangle > \langle \Omega(\mathcal{L})\rangle$ in 37, $\left\langle \Omega\left(\mathcal{L}^{1/4}\right)\right\rangle > \langle \Omega(\mathcal{L})\rangle$ in 41 and $\left\langle \Omega\left(\mathcal{L}^{1/100}\right)\right\rangle > \langle \Omega(\mathcal{L})\rangle$ in 48 of the networks analyzed (see figure 4(b)). That is, less than a half of the real-world networks studied here would benefit (in terms of the commute time) on the use of fractional random walks in comparison with local (standard) one.

We now consider $\left\langle \Omega\left(\tilde{\mathcal{L}}_s\right)\right\rangle$ for both series of graphs considered before. In the case of the 11 117 connected graphs with 8 nodes we observe that $\left\langle \Omega\left(\tilde{\mathcal{L}}_s\right)\right\rangle < \langle \Omega(\mathcal{L})\rangle$ in 11 116 graphs for $s = \{3, 2, 1\}$ and both indices are identical for the complete graph. Also, for 100% of the real-world networks studied here the average commute time based on the path Laplacian is smaller than that based on the local (and on fractional) Laplacian. That is, in terms of the commute time, the process based on path Laplacian is more efficient than those based on the local and on the fractional Laplacians. The fact that $\left\langle \Omega\left(\tilde{\mathcal{L}}_s\right)\right\rangle < \langle \Omega(\mathcal{L})\rangle$ for any graph can be proved as follows. Let $G = (V, E)$ be a simple connected graph different from the complete graph. Let $\tilde{\mathcal{L}}_s(G)$ be the path Laplacian of G. Then, $\tilde{A}_s$ is the adjacency matrix of a weighted complete graph $\tilde{K}_n$. It is known that $Kf(\mathcal{L})$ is a nonincreasing function of edge weights [59]. Then, if we reduce the weights of the edges the Kirchhoff index of the graph will not decrease. Because $\mathcal{L}(G) = \lim_{s\to\infty} \tilde{\mathcal{L}}_s(G)$, we have

$$Kf(\mathcal{L}(G)) \geqslant Kf\left(\tilde{\mathcal{L}}_s(G)\right). \tag{4.14}$$

In closing, for any graph different from the complete graph the path Laplacian produces a random walk with smaller average commute time than the process based on the standard Laplacian. In the case of the complete graphs both processes produce the same average commute time, which is the smallest possible one.

4.5. Diffusive efficiency

To measure the efficiency of local and nonlocal diffusive processes in a graph we consider the following metric [60]:

$$\Gamma_{pq}(\mathscr{L}) := \left(\mathrm{e}^{-\zeta\mathscr{L}}\right)_{pp} + \left(\mathrm{e}^{-\zeta\mathscr{L}}\right)_{qq} - 2\left(\mathrm{e}^{-\zeta\mathscr{L}}\right)_{pq}, \tag{4.15}$$

where $\mathscr{L} = \left\{L, L^{\alpha}, \tilde{L}(s)\right\}$ and $\zeta \in \mathbb{R}^{+}$ is a parameter. First we show that this metric is a Euclidean distance between the corresponding pair of nodes. Let $\mathscr{L} = U^{\mathrm{T}}\Lambda U$. Let φ_p be the pth column of U^{T}. Then, $\left(e^{-\zeta\mathscr{L}}\right)_{pq} = \varphi_p^{\mathrm{T}} e^{-\zeta\Lambda}\varphi_q = \left(e^{-\zeta\Lambda/2}\varphi_p\right)^{\mathrm{T}}\left(e^{-\zeta\Lambda/2}\varphi_q\right)$. Therefore, if $z_p := e^{-\zeta\Lambda/2}\varphi_p$, we can write

$$\begin{aligned}\Gamma_{pq}(\mathscr{L}) &= z_p \cdot z_p + z_q \cdot z_q - 2z_p \cdot z_q \\ &= \left\|z_p - z_q\right\|^2.\end{aligned} \tag{4.16}$$

Then, we have three Euclidean distances between the same pair of nodes: $\Gamma_{pq}(\mathcal{L})$, $\Gamma_{pq}(\mathcal{L}^{\alpha})$ and $\Gamma_{pq}(\mathcal{L}_s)$. Let us now explain how this measure captures the efficiency of a diffusive process. Let us consider the solution of the diffusion equation on graphs with initial condition $x_0(p) = 1$ and $x_0(r) = 0$ for all $r \neq p$. That is $x(t) = \exp(-t\mathscr{L})x_0 = \left[\left(e^{-t\mathscr{L}}\right)_{1p}, \left(e^{-t\mathscr{L}}\right)_{2p}, \ldots, \left(e^{-t\mathscr{L}}\right)_{np}\right]^{\mathrm{T}}$. Then, the concentration of the diffusive particle 'retained' at the node p is given by $\left(e^{-t\mathscr{L}}\right)_{pp}$ and that transferred to the node q is given by $\left(e^{-t\mathscr{L}}\right)_{qp}$. Thus, the efficiency of diffusing particles from p to q is $\left(e^{-t\mathscr{L}}\right)_{pp} - \left(e^{-t\mathscr{L}}\right)_{qp}$. If we do the same for the diffusion from q to p we get $\left(e^{-t\mathscr{L}}\right)_{qq} - \left(e^{-t\mathscr{L}}\right)_{pq}$. Therefore, because in an undirected network we have that $\left(e^{-t\mathscr{L}}\right)_{qp} = \left(e^{-t\mathscr{L}}\right)_{pq}$, the global efficiency of diffusing between p and q is $\Gamma_{pq}(\mathscr{L})$.

We use here the same series of graphs as in the previous section. In this case the results are more dramatic than for the case of the commute time. Here in 100% of the 11 117 connected graphs with 8 nodes we observe that $\langle \Gamma(\mathcal{L})\rangle < \langle \Gamma(\mathcal{L}^{\alpha})\rangle$ ($\alpha = 3/4, 1/2, 1/4, 1/100$). That is, the local diffusive process is always

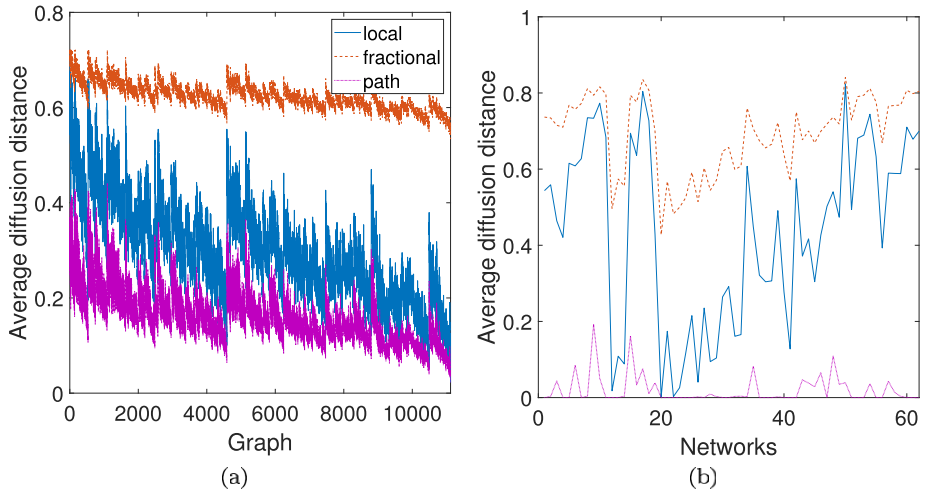

Figure 5. Plot of the average diffusive distance of all connected graphs with 8 nodes (a) and of 62 real-world networks (b). The 62 real-world networks represent a wide variety of complex systems, e.g. social, ecological, biomolecular, infrastructural and informational (see appendix in [9] for description and references). The continuous (blue) line corresponds to the distance based on local (standard) Laplacian, the broken (red) line to the one based on the fractional Laplacian and the dotted (magenta) line to the one based on the path Laplacian.

more efficient than the fractional one for all these graphs. When we study the 62 real-world networks previously considered we see that $\langle \Gamma(\mathcal{L})\rangle < \left\langle \Gamma\left(\mathcal{L}^{3/4}\right)\right\rangle$ in 61 of the networks. For values of $\alpha = \{0.5, 0.25, 0.01\}$ we observe that $\langle \Gamma(\mathcal{L})\rangle < \langle \Gamma(\mathcal{L}^{\alpha})\rangle$ in the 62 networks. On the other side of the coin we have that $\left\langle \Gamma\left(\tilde{\mathcal{L}}_s\right)\right\rangle < \langle \Gamma(\mathcal{L})\rangle$ $(s = \{3, 2, 1\})$ for all graphs with 8 nodes as well as for the real-world networks. Thus, again, the diffusive process controlled by the path Laplacian is more efficient than that controlled by the local (standard) Laplacian as well as by the fractional powers of it. The results are illustrated in figure 5.

5. Analysis of diffusion in brain cellular tissues

Here we propose to use local and nonlocal (fractional and path) diffusive dynamics to study the diffusion of a 'substance' through the cells in brain tissues. These tissue samples were surgically removed from different human brains from 12 different patients. They are grouped into three classes: healthy, inflamed and gliomas. Each image is taken with a magnification of 80× and consists of 384 × 384 pixels. Following Waxman [61], Gunduz *et al* [62] transformed these images into 'cell graphs' in which the nodes correspond to the cells in the tissue and the edges between them are based on a decaying exponential function of the Euclidean distance between every pair of cells (see [64] for a review). In figure 6 we illustrate three images corresponding to healthy, inflamed and cancerous tissues. We also illustrate the cell graphs constructed by Gunduz *et al* [62]. As can seen it is relatively easy to distinguish even by naked eye between healthy and unhealthy (inflamed and cancerous) tissues. The graphs of the first are very sparse and consist of several connected components. Here we always consider the largest connected component of these graphs.

The goal of this study is twofold. On one hand, we are interested in analyzing the capacity of local and nonlocal diffusive processes to classify these tissues into their corresponding classes. The importance of this experiment is understood by the fact that in clinical practice, the distinction between inflammation and glioma can be a difficult task [63]. It is known that in some cases, laboratory tests are atypical and clinical symptoms and signs of both pathologies are similar [63]. On the other hand, we would like to gain some insights about possible (diffusive) mechanisms taking place on these tissues which may illuminate about their main functional differences.

We then study 90 cell graphs (30 of healthy, 30 of inflamed and 30 of glioma tissues). For every graph we calculate the local and nonlocal (fractional and path) commute times as well as the corresponding diffusive distances. Our main goal here is to see whether there are significant differences between the local and nonlocal diffusive processes in the three kinds of tissues studied such that we can (i) differentiate them as well as (ii) gain some insight about different mechanisms acting on them. For this we produce scatterplots of the local and nonlocal diffusion distances of all the tissues studied. In figures 7(a)–(c) we show the violin plots of the average commute times for the three classes of cell graphs studied. The mean values of $\langle \Omega(\mathcal{L})\rangle$ are 4.240 for healthy, 1.357 for inflamed and 1.776 for glioma. Those for $\left\langle \Omega\left(\mathcal{L}^{0.25}\right)\right\rangle$ are 1.691, 1.510, and

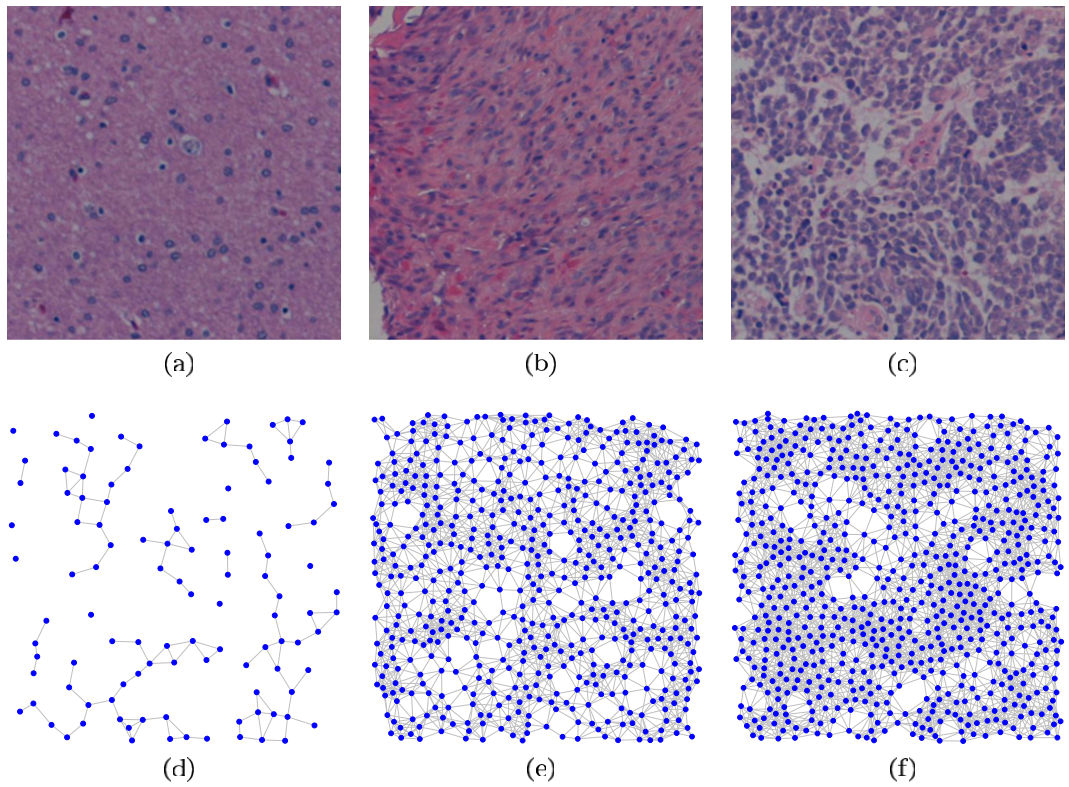

Figure 6. Microscopic images of tissue samples surgically removed from human brain (a)–(c) and the corresponding cell graphs (d)–(f): (a), (d) healthy, (b), (e) inflamed and (c), (f) a brain tumor sample (i.e. glioma).

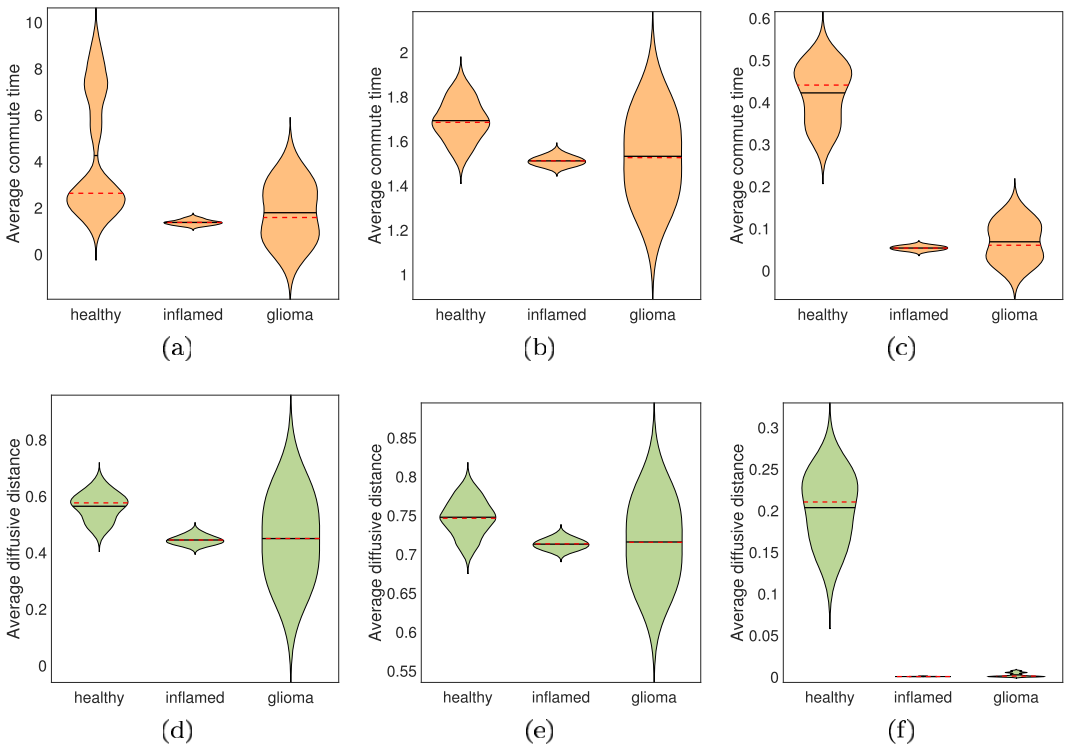

Figure 7. Violin plots of the average commute time (a)–(c) and of the average diffusive distance (d)–(f) calculated by the local (a), (d), fractional (b), (e) and path Laplacian (c), (f) for healthy, inflamed and glioma tissues.

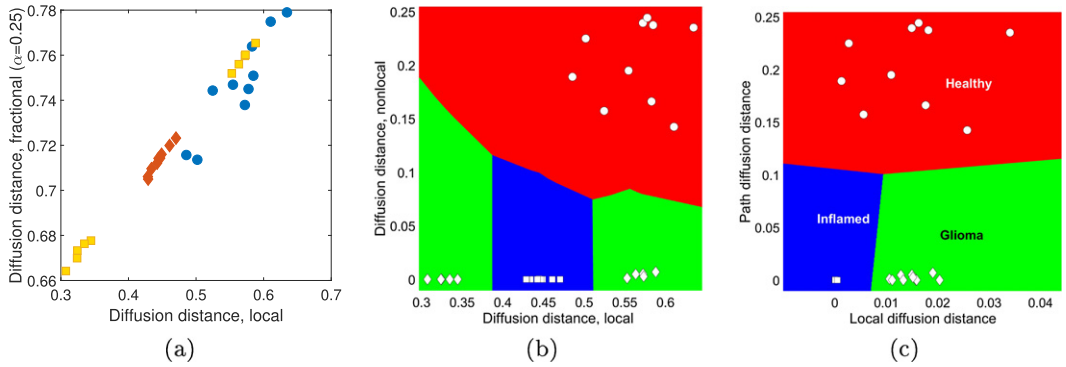

Figure 8. (a) Scatterplot of local $\langle \Gamma(\mathcal{L}) \rangle$ vs fractional $\langle \Gamma(\mathcal{L}^{\alpha}) \rangle$ diffusive distance ($\alpha = 1/4$) for all cell graphs analyzed here (blue circles: healthy; red diamonds: inflamed; yellow squares: glioma). (b) Visualization of the KNN clustering of healthy (circles), inflamed (squares) and glioma (diamonds) cellular tissues using diffusion distances based on local $\langle \Gamma(\mathcal{L}) \rangle$ (x-axis) and path $\left\langle \Gamma\left(\tilde{\mathcal{L}}(s)\right) \right\rangle$ (y-axis) diffusive models. The regions delimited by KNN for the classification are colored in red (healthy), blue (inflamed) and green (glioma). (c) The same as in (b) but using $\left(\langle \Gamma(\mathcal{L}) \rangle - 0.45\right)^2$ instead of $\langle \Gamma(\mathcal{L}) \rangle$ and the separation of classes is based on LDA.

1.531, respectively. Finally, for $\left\langle \Omega\left(\tilde{\mathcal{L}}_{s=2}\right) \right\rangle$ these values are 0.190, 0.088, and 0.102, respectively. Neither of the three kinds of commute times (local, fractional and path) produce a good separation of the three classes. Only, the path Laplacians produces a good separation of health and unhealthy tissues, but does not work well for the separation of inflamed and glioma. Interestingly, for the three classes the average commute times from the path Laplacians are significantly smaller than those based on fractional or local ones. The fractional Laplacian produces average commute time smaller than those obtained by the local operator for healthy and glioma tissues but not for the inflamed ones.

We then perform a similar analysis using the average diffusive distances. Here the averages of the diffusive distances for the three classes (healthy, inflamed and glioma) are: 0.563, 0.443, and 0.448 for the local operator, 0.747, 0.713, and 0.715 for the fractional, and 0.203, 8.47×10^{-5}, and 0.0021 for the path Laplacians. The fractional Laplacian always produces larger commute times than the local operator, while the path Laplacian produces always the smallest values of this parameter.

In figure 8(a) we illustrate the plot of the local versus the fractional diffusion distance. The first surprising observation is the extremely high linear correlation between both distances, which displays a Pearson correlation coefficient of 0.98. This means that 96% of the variance in the fractional diffusion distance is explained by the local diffusive one. In other words, it seems like if the fractional diffusive process does not bring any qualitatively new phenomenon into these tissues. Then (see figure 8(a)) the combination of these two variables is not able to differentiate the three classes of tissues studies here. In fact, healthy and part of the cancerous tissues are mixed up, but also some healthy tissues display similar fractional distances as the inflamed ones.

We now consider the plot of local and path diffusion distances for the same set of tissues as illustrated in figure 8(b). The Pearson correlation coefficient between these two variables is only 0.59, indicating that less than 35% of the variance in the nonlocal distance is accounted for by the local one. In other words, the new diffusive process introduces significantly different qualitative phenomena in relation to the local one. The second important characteristic observed in figure 8(b), where we show the classification made by K-nearest neighbors (KNN) as implemented in Matlab, is the fact that there is a clear separation between the three groups of tissues according to these two distances. First, the healthy and unhealthy tissues are well separated by the path diffusion distance, where the healthy tissues display significantly larger average path diffusion distances than the unhealthy ones. The inflamed tissues are separated into two classes, those displaying relatively low local diffusive distance and others displaying relatively large one. In the middle we find the glioma tissues. This indicates a quadratic separation of the inflamed and glioma tissues based on the local distance. That is, if we consider $\left(\langle \Gamma(\mathcal{L}) \rangle - 0.45\right)^2$ instead of $\langle \Gamma(\mathcal{L}) \rangle$ we reach a clear separation of the three classes as illustrated in figure 8(c). Therefore, the first goal, i.e. that of classifying the three classes of tissues, has been fulfilled. The percentage of good classification is 100% using simply linear discriminant analysis (LDA) classification.

We now focus on the potential meaning of our results. The first observation is that nonlocal diffusive processes controlled by the fractional Laplacian are not able to describe what is happening in these tissues, while the path Laplacian describes some effects that allows the differentiation of the three kinds of tissues. This may imply that some kind of non-backtracking processes are taking place in these tissues, particularly

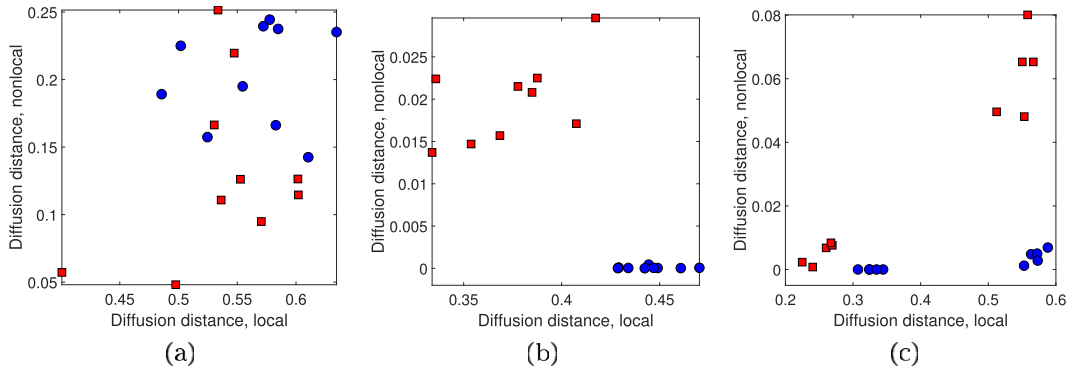

Figure 9. Plot of the average diffusion distances (local and nonlocal) between every pair of nodes in the cellular graphs (blue circles) of healthy (a), inflamed (b) and glioma (c) tissues. The average diffusion distances of the same graphs with a complete random rewiring of edges are plotted as red squares.

in unhealthy ones. One example of such kind of diffusive process is the 'through-space' one, as we have described before. In the case of cellular tissues this can be explained by the existence of 'transporters' that can move substances from one cell to another outside the cellular network. This is the case of exosomes, which are nano-vesicles used as vehicles to transfer proteins, lipids and nucleic acids from one cell to another. Exosomes are secreted by glioma cells facilitating the transport of receptors, signaling molecules, oncogenic genes and miRNA [65]. They are currently recognized as key components in the biogenesis of gliomas, which modify their surrounding microenvironment to support tumor progression. In addition, exosomes play a fundamental role in inflammatory processes [66], such as in the transport of pro-inflammatory cytokines.

We now search for indirect evidence about the role played by the structure of the cellular graphs on the behavior of both local and nonlocal diffusive processes. Hereafter we will only focus on the path Laplacian as the nonlocal process. With this goal in mind we perform randomization of the cell graphs, such that we rewire their edges by keeping the degree of the nodes. We then calculate $\langle \Gamma(\mathcal{L}) \rangle_{\text{rnd}}$ and $\left\langle \Gamma\left(\tilde{\mathcal{L}}_s\right) \right\rangle_{\text{rnd}}$ as the average of 100 random rewiring. In figure 9 we illustrate the results for the three classes of tissues studied.

As can be seen in figure 9(a) the random rewiring of the cells graphs of healthy tissues makes difficult to distinguish the real (blue circles) from the random (red squares) graphs. However, statistically the nonlocal diffusive distance of the real networks are bigger than those of the random ones (see table 1), indicating a relative small diffusive efficiency of the real networks to nonlocal processes. In the case of inflamed tissues the randomization destroys completely the structural characteristics of these cell graphs which produce the observed diffusive behavior. In particular, the inflamed tissues display slightly worse local 'diffusive efficiency', i.e. longer distances, than their random analogues as can be seen by the mean distances in table 1. However, they are significantly more efficient than the random ones in the nonlocal diffusion. In other words, it seems like if the inflamed tissues produce certain structural patterns which increase their efficiency for nonlocal diffusion in detriment of the local one. Finally, in the case of gliomas we see again the separation previously observed in figure 8(b). There is a subgroup (hereafter named subgroup I) located at the left-bottom part of the plot, which have slightly less diffusive efficiency than the random analogues (see table 1) but with a significant improvement of their nonlocal diffusive efficiency. The second subgroup (labeled II in table 1), which is located at the right-bottom part of the plot, has approximately the same diffusive capacity as the randomized ones, but displaying a significant improvement in their nonlocal diffusive efficiency.

As can be seen in figure 8(b) the networks representing healthy tissues are the ones where nonlocal diffusion produces the least improvement in the diffusion efficiency (measured by the diffusion distances) in relation to the local one. This means that in healthy tissues local diffusive processes reach efficiencies which are comparable to the nonlocal ones, i.e. the ratio of the nonlocal to local diffusive distance is less than 3. In the cases of unhealthy tissues this change is dramatic. For instance, the ratio of the local to nonlocal diffusive distance in the glioma (group II) is 139, in glioma (group I) is 4853 and in inflamed is almost 2 millions. These results indicate that in these tissues the presence of nonlocal diffusive mechanisms will benefit the efficiency of the processes in extremely high proportions in relation to local processes.

Finally, we speculate about the possible reasons for the separation of the glioma tissues into two separated classes. Unfortunately, we do not have clinical details about the kinds of gliomas corresponding to

Table 1. Values of the average diffusive distance based on local and path Laplacians for the cell graphs of health, inflamed and glioma tissues, as well as their randomized versions. The glioma tissues are subdivided into two subgroups (see text for details). The probability that the difference between the two means is significant at 95% of confidence is calculated based on the two-samples *t*-test.

	$\mathcal{L}$			$\mathcal{L}_{s=2}$		
	Real	Rand.	$p\,(95\%)$	Real	Rand.	$p\,(95\%)$
Healthy	0.563	0.539	0.7092	0.203	0.139	**0.9892**
Inflamed	0.445	0.374	**1.0000**	9.17×10^{-5}	0.020	**1.0000**
Glioma (I)	0.327	0.252	**0.9998**	1.71×10^{-7}	0.005	**0.9904**
Glioma (II)	0.57	0.55	0.9168	0.0041	0.062	**1.0000**

each of the tissues. According to the World Health Organization (WHO), gliomas are classified into four grades, which represents the overall malignant potential of the tumor [67–69]. In particular, the differentiation between low-grade gliomas (grade II) and high-grade gliomas (grades III, IV) is extremely important for the prognosis and the therapeutic strategy to follow. While WHO grades I and II gliomas are slow growing [67], WHO grade III gliomas are rapidly growing [67]. Therefore, we think that the separation observed would correspond with the separation between low- and high-grade gliomas due to their different growing mechanisms and histopathologic characteristics. More data and experiments are needed to falsify this hypothesis.

6. Conclusions

From the current investigation of the two nonlocal Laplacian operators for networks, i.e. fractional and path Laplacian, we can conclude the following.

- Path-based nonlocal diffusion always converges faster than, or at the same rate as, the local diffusion.
- Fractional nonlocal diffusion converges slower than the local process if the algebraic connectivity of the graph is not smaller than one, which is frequently the case.
- Fractional Laplacians describe backtracking processes on graphs. Consequently, the diffusion can get trapped between the initial node and an obstacle located at another node, such as a self-loop.
- Path Laplacians describe non-backtracking jumps, which may represent through-space navigation in the graphs, which overcome obstacles as the ones before mentioned.
- Fractional diffusion frequently has longer commute times and worse diffusive efficiency than the standard diffusion process.
- Path-based diffusion always produces smaller commute times and better diffusive efficiencies than the standard diffusion.
- Diffusive processes based on path Laplacians are able to classify correctly 100% of cellular brain samples from healthy, inflamed and glioma, but such classification was not possible using diffusive processes based on the fractional Laplacian.

Acknowledgments

The author thanks Professor Bülent Yener (Rensselaer Polytechnic Institute) for the cell cancer datasets, the tissue images illustrated in figure 6 as well as for useful discussions about this topic. Revision of a former version of the manuscript as well as useful comments and discussions about the two classes of nonlocal Laplacians studied here are also thanked to Professor Michele Benzi (Scuola Normale Superiore di Pisa). The author thanks financial support from Ministerio de Ciencia, Innovacion y Universidades, Spain for the Grant PID2019-107603GB-I00 'Hubs-repelling/attracting Laplacian operators and related dynamics on graphs/networks'.

Data availability statement

The data that support the findings of this study are available upon reasonable request from the authors.

Appendix.

See figures 10 and 11

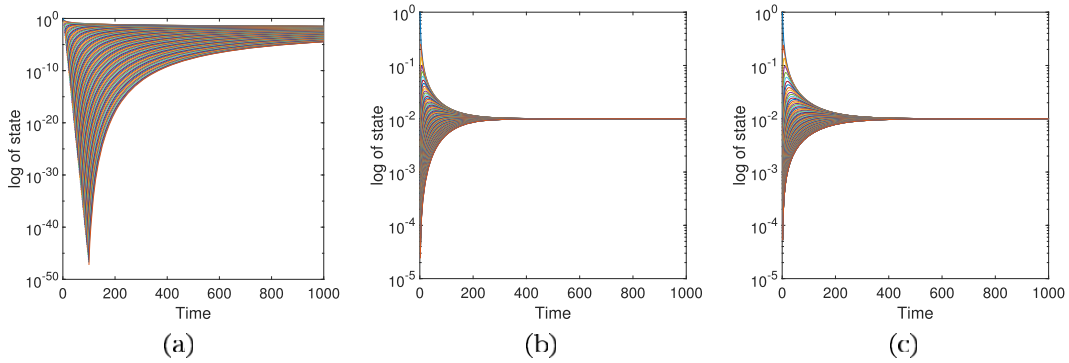

Figure 10. Time evolution of the state (concentration) of a diffusive particle at the different nodes of a linear chain with 100 nodes. The plots correspond to the use of the three different Laplacian $\mathcal{L}$ (a), $\mathcal{L}^{1/2}$ (b) and $\tilde{\mathcal{L}}_{s=2}$ (c). Notice that for the standard Laplacian (a) the convergence is reached for $t > 1000$. Also notice that in the cases of the local Laplacian (a) at times $t < 100$ there are nodes which have not been visited by the particle, e.g. its concentrations are close to zero at rounding error of Matlab. This is not the case for the nonlocal Laplacians were such concentrations are about 10^{-4} for very early times.

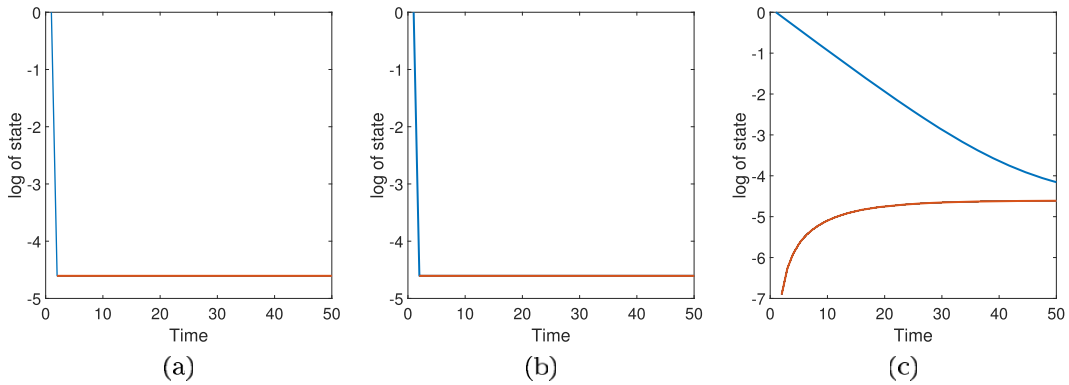

Figure 11. Time evolution of the state (concentration) of a diffusive particle at the different nodes of a complete graph with 100 nodes. The plots correspond to the use of the three different Laplacian $\mathcal{L}$ (a), $\mathcal{L}^{1/2}$ (b) and $\tilde{\mathcal{L}}_{s=2}$ (c). Notice that for $\mathcal{L}$ (a), and $\tilde{\mathcal{L}}_{s=2}$ (c) the convergence is immediately at $t = 1$. This is not the case for the $\mathcal{L}^{1/2}$ where the steady state is only reached at $t > 50$.

ORCID iDs

Ernesto Estrada https://orcid.org/0000-0002-3066-7418

References

[1] Yu C, Guan J, Chen K, Bae S C and Granick S 2013 Single-molecule observation of long jumps in polymer adsorption *ACS Nano* **7** 9735–42
[2] Ala-Nissila T, Ferrando R and Ying S C 2002 Collective and single particle diffusion on surfaces *Adv. Phys.* **51** 949–1078
[3] King A E and Turner M S 2021 Non-local interactions in collective motion *R. Soc. Open Sci.* **8** 201536
[4] Chen L, Painter K, Surulescu C and Zhigun A 2020 Mathematical models for cell migration: a non-local perspective *Phil. Trans. R. Soc.* B **375** 20190379
[5] Ninomiya H, Tanaka Y and Yamamoto H 2017 Reaction, diffusion and non-local interaction *J. Math. Biol.* **75** 1203–33
[6] Balagué D, Carrillo J A, Laurent T and Raoul G 2013 Nonlocal interactions by repulsive-attractive potentials: radial ins/stability *Physica* D **260** 5–25
[7] Boccaletti S, Latora V, Moreno Y, Chavez M and Hwang D 2006 Complex networks: structure and dynamics *Phys. Rep.* **424** 175–308

[8] Newman M E J 2003 The structure and function of complex networks *SIAM Rev.* **45** 167–256
[9] Estrada E 2012 *The Structure of Complex Networks: Theory and Applications* (Oxford: Oxford University Press)
[10] Santos L F, Borgonovi F and Celardo G L 2016 Cooperative shielding in many-body systems with long-range interaction *Phys. Rev. Lett.* **116** 250402
[11] Bachelard R, Chandre C, Fanelli D, Leoncini X and Ruffo S 2008 Abundance of regular orbits and nonequilibrium phase transitions in the thermodynamic limit for long-range systems *Phys. Rev. Lett.* **101** 260603
[12] Lischke A *et al* 2020 What is the fractional Laplacian? A comparative review with new results *J. Comput. Phys.* **404** 109009
[13] Gilboa G and Osher S 2009 Nonlocal operators with applications to image processing *Multiscale Model. Simul.* **7** 1005–28
[14] Estrada E 2012 Path Laplacian matrices: introduction and application to the analysis of consensus in networks *Linear Algebr. Appl.* **436** 3373–91
[15] Estrada E, Hameed E, Hatano N and Langer M 2017 Path Laplacian operators and superdiffusive processes on graphs. I. One-dimensional case *Linear Algebr. Appl.* **523** 307–34
[16] Estrada E, Hameed E, Langer M and Puchalska A 2018 Path Laplacian operators and superdiffusive processes on graphs. II. Two-dimensional lattice *Linear Algebr. Appl.* **555** 373–97
[17] Riascos A P and Mateos J L 2012 Long-range navigation on complex networks using Lévy random walks *Phys. Rev.* E **86** 056110
[18] Riascos A P and Mateos J L 2014 Fractional dynamics on networks: emergence of anomalous diffusion and Lévy flights *Phys. Rev.* E **90** 032809
[19] Estrada E and Vargas-Estrada E 2013 How peer pressure shapes consensus, leadership and innovations in social groups *Sci. Rep.* **3** 1–6
[20] Estrada E, Gambuzza L V and Frasca M 2018 Long-range interactions and network synchronization *SIAM J. Appl. Dyn. Syst.* **17** 672–93
[21] Zhang Y, Zhang X and Liu K 2020 Weight allocation in Laplacian matrix of random networks based on geodesic distances *Int. J. Syst. Sci.* **51** 1266–79
[22] Fang R, Wang X, Su H and Xiao M 2021 The variant *d*-path Laplacian based consensus protocols for networked harmonic oscillators *Neurocomputing* **422** 277–86
[23] Tlaie A, Leyva I and Sendiña-Nadal I 2019 High-order couplings in geometric complex networks of neurons *Phys. Rev.* E **100** 052305
[24] Estrada E, Estrada-Rodriguez G and Gimperlein H 2020 Metaplex networks: influence of the exo-endo structure of complex systems on diffusion *SIAM Rev.* **62** 617–45
[25] Riascos A P and Mateos J L 2017 Emergence of encounter networks due to human mobility *PloS One* **12** e0184532
[26] Michelitsch T M, Collet B A, Riascos A P, Nowakowski A F and Nicolleau F C G A 2017 Fractional random walk lattice dynamics *J. Phys. A: Math. Theor.* **50** 055003
[27] Riascos A P and Mateos J L 2015 Fractional diffusion on circulant networks: emergence of a dynamical small world *J. Stat. Mech.* P07015
[28] Riascos A P, Michelitsch T M and Pizarro-Medina A 2020 Nonlocal biased random walks and fractional transport on directed networks *Phys. Rev.* E **102** 022142
[29] Benzi M, Bertaccini D, Durastante F and Simunec I 2020 Non-local network dynamics via fractional graph Laplacians *J. Complex Netw.* **8** cnaa017
[30] Merris R 1994 Laplacian matrices of graphs: a survey *Linear Algebr. Appl.* **197–198** 143–76
[31] Mohar B 1991 The Laplacian spectrum of graphs *Graph Theory, Combinatorics, and Applications* vol 2 ed Y Alavi, G Chartrand, O R Oellermann and A J Schwenk (New York: Wiley) pp 871–98
[32] Grone R, Merris R and Sunder V S 1990 The Laplacian spectrum of a graph *SIAM J. Matrix Anal. Appl.* **11** 218–38
[33] Grone R and Merris R 1994 The Laplacian spectrum of a graph II *SIAM J. Discrete Math.* **7** 221–9
[34] Lovász L 1993 *Random walks on graphs: A Survey Combinatorics, Paul Erdös is Eighty* vol 2 (Hungary: Bolyai Society Mathematical Studies) pp 1–46
[35] Aldous D and Fill J *Reversible Markov Chains and Random Walks on Graphs* in preparation https://stat.berkeley.edu/aldous/RWG/book.pdf
[36] Coppersmith D, Feige U and Shearer J 1996 Random walks on regular and irregular graphs *SIAM J. Discrete Math.* **9** 301–8
[37] Masuda N, Porter M A and Lambiotte R 2017 Random walks and diffusion on networks *Phys. Rep.* **716–717** 1–58
[38] Ghedini C, Ribeiro C H and Sabattini L 2016 Improving the fault tolerance of multi-robot networks through a combined control law strategy *8th Int. Workshop on Resilient Networks Design and Modeling. (RNDM)* (13 Sep 2016) (Piscataway, NJ: IEEE) pp 209–15
[39] De Abreu N M M 2007 Old and new results on algebraic connectivity of graphs *Linear Algebr. Appl.* **423** 53–73
[40] Fiedler M 1973 Algebraic connectivity of graphs *Czech. Math. J.* **23** 298–305
[41] Fiedler M 1989 Laplacian of graphs and algebraic connectivity *Banach Center Publ.* **25** 57–70
[42] Mugnolo D 2014 *Semigroup Methods for Evolution Equations on Networks* (Berlin: Springer)
[43] Tatsuoka F, Sogabe T, Miyatake Y, Kemmochi T and Zhang S L 2020 Computing the matrix fractional power with the double exponential formula (arXiv:2012.01667)
[44] Erdös P and Rényi A 1960 On the evolution of random graphs *Publ. Math. Inst. Hung. Acad. Sci.* **5** 17–60
[45] Juhász F 1991 The asymptotic behaviour of Fiedler's algebraic connectivity for random graphs *Discrete Math.* **96** 59–63
[46] Joswig M and Schröter B 2019 The tropical geometry of shortest paths (arXiv:1904.01082)
[47] Hook J 2017 Min-plus algebraic low rank matrix approximation: a new method for revealing structure in networks (arXiv:1708.06552)
[48] Bouillard A, Boyer M and Le Corronc E 2018 *Deterministic Network Calculus: From Theory to Practical Implementation* (New York: Wiley)
[49] Olfati-Saber R and Murray R M 2004 Consensus problems in networks of agents with switching topology and time-delays *IEEE Trans. Autom. Control* **49** 1520–33
[50] Doyle P G and Snell J L 2000 Random walks and electric networks (arXiv:math/0001057)
[51] Klein D J and Randić M 1993 Resistance distance *J. Math. Chem.* **12** 81–95
[52] Palacios J L 2001 Resistance distance in graphs and random walks *Int. J. Quant. Chem.* **81** 29–33
[53] Xiao W and Gutman I 2003 Resistance distance and Laplacian spectrum *Theor. Chim. Acta* **110** 284–9
[54] Ghosh A, Boyd S and Saberi A 2008 Minimizing effective resistance of a graph *SIAM Rev.* **50** 37–66

[55] Ellens W, Spieksma F M, Van Mieghem P, Jamakovic A and Kooij R E 2011 Effective graph resistance *Linear Algebr. Appl.* **435** 2491–506
[56] Zhou B and Trinajstić N 2009 On resistance-distance and Kirchhoff index *J. Math. Chem.* **46** 283–9
[57] Palacios J L 2001 Closed-form formulas for Kirchhoff index *Int. J. Quantum Chem.* **81** 135–40
[58] Das K C 2013 On the Kirchhoff index of graphs *Z. Naturforsch. A.* **68** 531–8
[59] Tizghadam A and Leon-Garcia A 2009 Autonomic traffic engineering for network robustness *IEEE J. Selec. Areas Comm.* **28** 39–50
[60] Fouss F, Francoisse K, Yen L, Pirotte A and Saerens M 2012 An experimental investigation of kernels on graphs for collaborative recommendation and semisupervised classification *Neural Netw.* **31** 53–72
[61] Waxman B M 1988 Routing of multipoint connections *IEEE J. Select. Areas Commun.* **6** 1617–22
[62] Gunduz C, Yener B and Gultekin S H 2004 The cell graphs of cancer *Bioinformatics* **20** i145–51
[63] Han Y *et al* 2021 Distinguishing brain inflammation from grade II glioma in population without contrast enhancement: a radiomics analysis based on conventional MRI *Eur. J. Radiol.* **134** 109467
[64] Gurcan M N, Boucheron L E, Can A, Madabhushi A, Rajpoot N M and Yener B 2009 Histopathological image analysis: a review *IEEE Rev. Biomed. Eng.* **2** 147–71
[65] Gourlay J, Morokoff A P, Luwor R B, Zhu H-J, Kaye A H and Stylli S S 2017 The emergent role of exosomes in glioma *J. Clin. Neurosci.* **35** 13–23
[66] Console L, Scalise M and Indiveri C 2019 Exosomes in inflammation and role as biomarkers *Clin. Chim. Acta* **488** 165–71
[67] Weller M *et al* 2015 Glioma *Nat. Rev. Dis. Prim.* **1** 1–8
[68] Gates E D H *et al* 2020 Imaging-based algorithm for the local grading of glioma *Am. J. Neuroradiol.* **41** 400–7
[69] Togao O *et al* 2015 Differentiation of high-grade and low-grade diffuse gliomas by intravoxel incoherent motion MR imaging *Neuro Oncol.* **18** 132–41